Estimation of Ionization Coefficients of Gallium Oxide for the Purpose of TCAD Simulation

BY

GIFTSONDASS IRUDAYADASS
B.E., Anna University, 2011

THESIS

Submitted as partial fulfillment of the requirements
for the degree of Master of Science in Electrical and Computer Engineering
in the Graduate College of the
University of Illinois at Chicago, 2018

Chicago, Illinois

Defense Committee:

Junxia Shi, Chair and Advisor
Michael Stroscio
Danilo Erricolo

To all my teachers...

ACKNOWLEDGMENTS

I would like to thank my advisor and committee members- Dr. Junxia Shi, Dr. Michael Stroscio, Dr. Danilo Erricolo,- for their unwavering support and guidance throughout my master's degree. I am immensely grateful to my defense committee to make every possible effort to accommodate my defense within their busy schedule.

I am grateful to Dr. Zheng Yang, Dr. Igor Paprotny, Dr. Rui Yang and the defense committee members for teaching courses that were relevant to my research at Electrical and Computer Engineering department. I would also like to acknowledge the members of the Advanced Compound Semiconductor Materials and Devices Lab namely, Xiaowei Wang, Yu Wen, Arnab Neogi and Miaozhen Mei for their suggestions and support.

A special thanks to Dr. Parijat Sengupta for his guidance and support.

I thank Dr. Sankar Padmanabhan for inspiring me to pursue thesis.

GI

TABLE OF CONTENTS

TABLE OF CONTENTS (Continued)

CHAPTER **PAGE**

LIST OF TABLES

LIST OF FIGURES

LIST OF ABBREVIATIONS

IIM	Impact Ionization Models.
BJT	Bi-polar junction transistor.
GaN	Gallium Nitride.
SiC	Silicon Carbide.
TCAD	Technology computer aided designing.
BFOM	Baliga's figure of merit.
InP	Indium Phosphide.
PFC	Power factor correction.
IGBT	Insulated gate bipolar transistor.
SBD	Schottky barrier diode.
UV	Ultra-violet.
AlN	Aluminium Nitride.
TCO	Transparent conducting Oxide.
LED	Light Emitting Diode.
FZ	Floating Zone technique.
CZ	Czochralski process.
EFG	Edge-defined film-fed growth.

LIST OF ABBREVIATIONS (Continued)

MBE	Molecular beam epitaxy.
HVPE	Halide Vapour phase epitaxy.
MOCVD	Metal-organic chemical vapour deposition.
TMG	Trimethylgallium.
MFP	Mean free path.

SUMMARY

Gallium Oxide is not a novel device, however its semiconducting properties have been ignored owing to two reasons, one being overshadowed by other compound materials like Gallium Nitride and Silicon carbide and the other pertaining to its use as a gas sensor, a transparent conducting oxide and oxides looked upon as dielectrics in general. Recent studies has proved the possible superior capability of Gallium Oxide in power semiconductor industry, by taking note of its excellent power related properties like, wide bandgap, large Baliga's figure of merit and high breakdown field. Though the spotlight has turned towards gallium oxide, numerous properties of it are still unknown and most of the known characteristics are based on first-principle, density functional theory simulations.

In this thesis, our primary goal is to estimate one such parameter of gallium oxide related to field effect transistor and power application, the impact ionization coefficients which plays an important role in device breakdown. We use several impact ionization models to estimate the coefficients and compare them with related semiconductor compound materials like Gallium Nitride and Silicon Carbide. An integral part of this estimation depends on the determination of the phonon mean free path, which can be derived from its relation to the thermal conductivity given by gray approximation. We also determine a critical multiplication limit below which the previously estimated values are valid depending on the boundary conditions but the models do not hold above this limit.

CHAPTER 1

INTRODUCTION

The power semiconductor industry dominated by the current Si-based technology has fallen short in satisfying the demands, leaving a void currently being filled by SiliconCarbide(SiC) and Gallium-Nitride(GaN) which possess desired power electronics specific material properties like large band gap (E_g) and high breakdown field (E_{br}), since a great deal of research and development was focussed on SiC and GaN power devices. Recently, by virtue of its extraordinary material properties like baliga's figure of merit $(BFOM)$ for β-Ga_2O_3 being larger than those of Si, SiC and GaN and its power device performance, Ga_2O_3 has gained focus as a semiconductor to fill the void and compete with SiC and GaN. Though bulk melt grown native substrates are available, they are higher-priced than silicon substrates currently used in the industry, which brings simulation tools into spotlight. TCAD Simulation tools help in reducing the cost while improving the quality of experimental research by highlighting device structures with desired output characteristics, but the majority of the tools and methods are oriented towards silicon based devices. While methods, models and coefficients are available for other materials like SiC, GaN and Indium Phosphide (InP), little to no data are available for Ga_2O_3. In this work we will determine such coefficients and desirable models to be used for β-Ga_2O_3, particularly the coefficients for impact ionization modelling since the major focus on β-Ga_2O_3 is for power applications.

Due to the lack of fundamental research, the estimation of impact Ionization coefficient depends on the determination of phonon mean free path and fortunately enough data is available to estimate this value. Phonon mean free path was calculated to be 5.2604, 3.0675, 2.99 and 2.736 Å, for crystallo-

graphic directions [010], [100], [001] and $[\bar{2}01]$, respectively. The impact Ionization rate constants were calculated using the standard impact ionization models (IIM) provided by Crowell-Sze, Sutherland and Thornber and these values were used in Selberherr IIM. The model suggested by Sutherland in Ref. (1) provides the best fit to Universal Baraff's Curve for ionization rates, and has the values 3.98×10^6, 7.626×10^6, 8.965×10^6 and 9.485×10^6 cm $^{-1}$ for crystallographic directions [010], [100], [001] and $[\bar{2}01]$.

1.1 Power and high voltage devices

The basic required property of a power semiconducting device is to withstand high voltages. These devices are pivotal pieces in many applications of which some are, switched mode power supplies, power factor correction (PFC) and motor control. This application was monopolized by devices like power bipolar junction transistors (BJT), insulated gate bipolar transistor (IGBT) and P-I-N diodes, which was recently challenged by unipolar devices like silicon carbide Schottky barrier diode (SiC-SBD). High voltage semiconducting devices are typically above 300 Volts, and to withstand such a high voltage the important properties to look for is the bandgap and breakdown field.

1.2 Why Gallium Oxide ?

The power related properties of β-Ga_2O_3 have been measured to be excellent and having a BFOM of 3444 (2) which is several orders higher that of most commercially available power semiconductor material and bettered only by diamond. β-Ga_2O_3 is naturally n-type, which is attributed to many reasons such as oxygen vacancies during the growth of the material or the presence of hydrogen in the chamber atmosphere influencing the increase of oxygen vacancies but the most significant reason accepted by most is the presence of silicon in the precursor used during the growth process. Though it is naturally

n-type the electrical conductivity is still low, which is one of the disadvantages of β-Ga_2O_3. The band gap of β-Ga_2O_3 is in the ultra-wide range, putting it out of the visible spectrum and into the UV region, hence this material finds UV optoelectronic and UV photodetector applications. It is also a transparent conducting oxide, being researched for flexible screen applications. But the major focus on β-Ga_2O_3 now is in the power electronic field, since BFOM, bandgap are high and adding to this its uses as a high frequency switching device in the GHz range has been recently noted.(3) Such a promising material with many desirable properties needs to be researched and commercialised so its potential can be used to the maximum.

CHAPTER 2

GALLIUM OXIDE : PROPERTIES

Most important property of Ga_2O_3 is its bandgap, and since growing single crystalline structures, various properties of Ga_2O_3 have been studied.

2.1 Polymorphism

Ga_2O_3 single crystals can form several different polymorphs (4) of which five are studied in detail, namely $\alpha, \beta, \gamma, \delta and \varepsilon$. Each polymorph has different space groups and different coordination of Gallium atoms and a polytype κ has also been noted in literature. The α polymorph can be synthesized heating gallium oxide hydroxide in the presence of oxygen at an average of 500° C and is rhombohedral belonging to space group No.167. The β polymorph belongs to the base-centered monoclinic structure. The γ polymorph belongs to space group No.227 and has a defective cubic spinel type structure. The δ polymorph is a nanocrystalline form of the ε polymorph and is not considered distinct though it exhibits a C-type rare earth structure. The ε polymorph was said to belong to space group No.33 through simulations but belongs to No.186. Not much information is known about the κ polymorph. Of all these polymorphs β is said to be most stable thermodynamically and chemically, hence we will focus our discussion on this polymorph.

2.2 Crystal Structure

β-Ga_2O_3 belongs to the base centered monoclinic structure and is placed in space group No.12, C2/m. This is the well researched and most common polymorph of them all, and is also the only

stable form of Ga_2O_3, both thermodynamically and chemically, for devices to be built from. This thermal stability has made it possible to grow β-Ga_2O_3 through melt based growth techniques similar to silicon through czochralski process and edge defined film fed growth. The other forms of growth for gallium oxide include, vapour phase epitaxy, metal-organic chemical vapour deposition, plasma enhanced chemical vapour deposition and so on. This has increased the availability of high quality crystals for the purpose of research and attracting more researchers towards this material.

The unit cell of β-Ga_2O_3, shown in Fig 1 (a), consists of two inequivalent Ga sites (large sphere), three inequivalent O-sites (small sphere) and contains a total of 30 atoms and the primitive cell represented comprises of 10 atoms, Fig 1(b) illustrates the tetrahedral and octahedral geometry of Ga1 and Ga2 sites respectively. The lattice parameters corresponding to the crystallographic axis of β-Ga_2O_3 unit cell are given as, a = 12.214 Å, b = 3.037 Å, c = 5.7981Å, and β = 103.83° (between a and c) (6), which implies that this crystal belongs to the C12/m1 space group for which the parallelpiped reciprocal lattice vector unit cell brillouin zone schematic is shown in Fig 3, (7; 8; 9; 10; 11) and a detailed brillouin zone computed using the primitive cell was suggested by H. Peelaers and C. G. Van de Walle (12). The dielectric constant of β-Ga_2O_3 was set to 10.2, as given in Refs. (13; 14). The angles between different bonds of the two Ga sites with respect to the O sites, the bond lengths and the geometrical representation of β-Ga_2O_3 is shown in Fig. 2.

2.3 Parallelpiped representation

The axial relation between the lattice parameters have several possibilities for monoclinic structure which leads to many brillouin zones which are topologically different from each other hence these can be replaced by the primitive cells which are parallelpipeds independent of axial relations. A schematic

containing the k-vectors of the unit cell and the asymmetric unit of the arithmetic class 2/mC is given in Fig. 3

2.4 Primitive Cell brillouin zone

The brillouin of β-Ga_2O_3 simulated form the primitive cell was presented by Peelaers et al. (12) The transformational axis for primitive cell from the conventional unit cell was given from,

$$a_1^{conv} = a\hat{x} + 0\hat{y} + 0\hat{z}, \tag{2.1a}$$

$$a_2^{conv} = 0\hat{x} + b\hat{y} + 0\hat{z}, \tag{2.1b}$$

$$a_3^{conv} = c\cos\beta\hat{x} + 0\hat{y} + c\hat{z}, \tag{2.1c}$$

as,

$$a_1^{prim} = (a_1^{conv} + a_2^{conv})/2, \tag{2.1d}$$

$$a_2^{prim} = (-a_1^{conv} + a_2^{conv})/2, \tag{2.1e}$$

$$a_3^{prim} = a_3^{conv}. \tag{2.1f}$$

where, conv denotes conventional and prim denotes primitive and $\hat{x}$, $\hat{y}$, $\hat{z}$ are the Cartesian coordinates and a_1, a_2 and a_3 are the crystallographic axis. The brillouin zone thus simulated is shown in Fig 4 (b) and the primitive cell from which it was derived is shown in Fig. 4 (a).

2.5 Band structure

The band structure simulated using the primitive cell structure shown in sec. 4 (a) is shown in Fig. 4(c). The zero temperature bandgap calculated from this structure was 4.84 eV, The valence band maximum is at the I-L line and the conduction band minimum is at Γ, which makes the bandgap of β-Ga_2O_3 an indirect bandgap. β-Ga_2O_3 is still effectively a direct bandgap material since the gap at Γ is 4.88 eV which is only a 0.04 eV difference from the indirect bandgap measured. The effective mass of electrons was also calculated by Peelaers et al., (12) as $0.28m_e$.

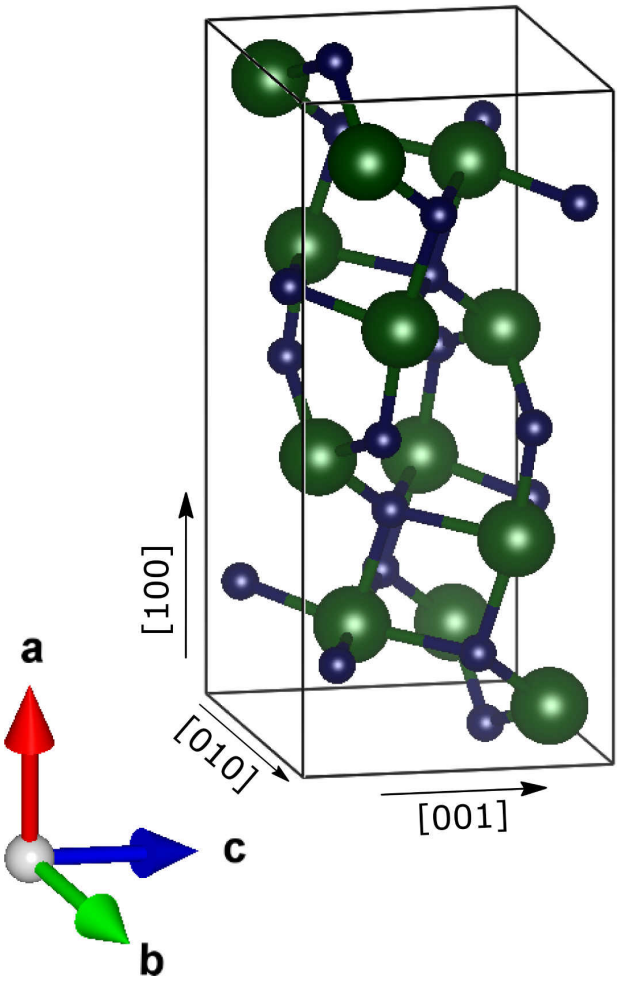

The simulated image represents the unit cell of β-Ga_2O_3 which consists of two inequivalent Ga sites (large spheres), three inequivalent O-sites (small spheres) and contains 20 atoms (4 Ga_2O_3). The lattice parameters (length, breadth and width of the unit cell along the crystallographic axis, and the corresponding angles) are given as, a = 12.214 Å, b = 3.037 Å, c = 5.7981Å, and β = 103.83° (between a and c) (5; 6).

Figure 1: Atomic unit cell.

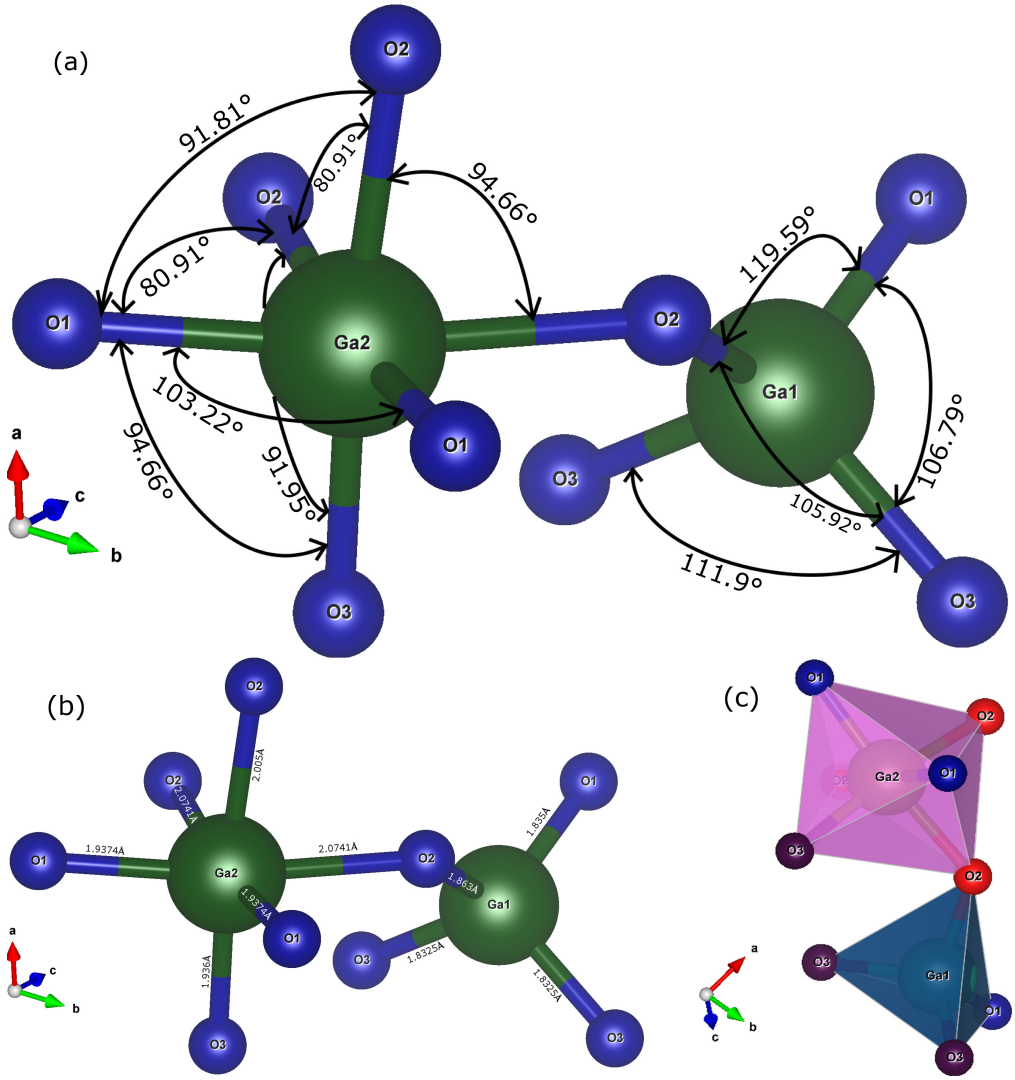

The figure on top (a) gives the angle between different bonds. The figure at the bottom left (b) gives the bond lengths and figure to the right (c) illustrates the tetrahedral and octahedral geometry of β-Ga_2O_3.

Figure 2: Selected geometry of β-Ga_2O_3.

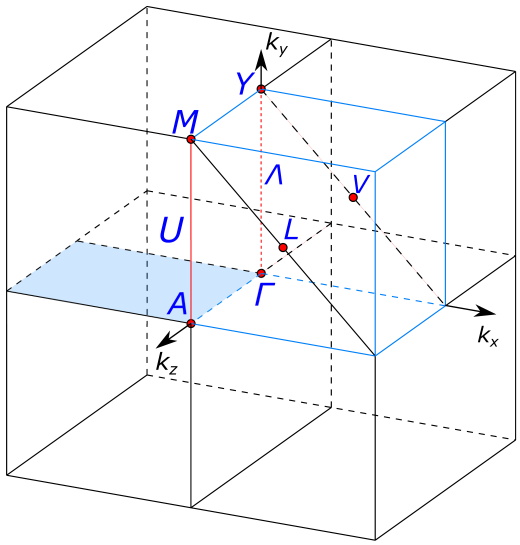

k-vectors of group C2/m to which β-Ga_2O_3 belongs, in its parallelpiped representation.

Figure 3: Unit cell and k-space representation of Space group 12.

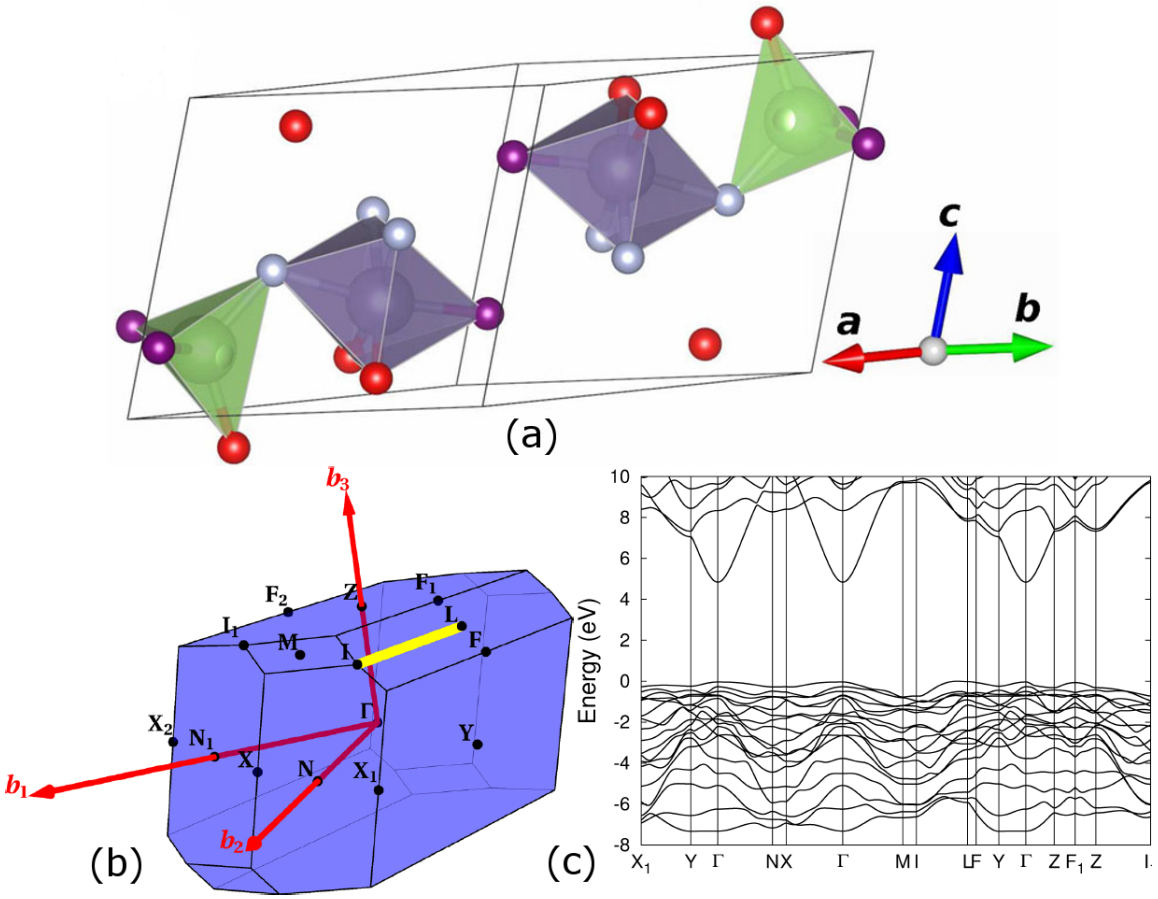

The brillouin zone (b) and energy band sketch (c) based on the primitive cell (a) derived by Peelaers et al.

Figure 4: Primitive Cell.

CHAPTER 3

GALLIUM OXIDE : CRYSTAL GROWTH

Gallium oxide was predominantly grown as a substrate for the fabrication of other semiconducting materials like GaN, Aluminium Nitride (AlN) and their alloys. Not until recently were techniques for the growth of single crystal Gallium oxides were perfected which led to its application as a electrical conducting device where as earlier it was used as a transparent conducting oxide (TCO) for light emitting diodes (LED). A major advantage of moving towards the use of gallium oxide for the purpose of electrical conduction device is the availability of melt grown single crystal substrates which can be grown in bulk and that too in standard atmospheric conditions. A number of melt based growth techniques have been developed for gallium oxide in the past few years, some of which are, Floating zone technique (FZ), Czochralski process (CZ), edge-defined film-fed growth (EFG) method. Other power semiconductors who are in competition with gallium oxide, like GaN or SiC cannot be grown through a melt, atleast not in standard atmospheric conditions.

Along with melt growth techniques, growth of homo-epitaxial thin film of gallium oxide have also been increasing in recent years. Gallium oxide is known to have grown using molecular beam epitaxy (MBE), halide vapoue phase epitaxy (HVPE), metalorganic chemical vapour deposition (MOCVD), mist chemical vapour deposition (Mist-CVD). We shall discuss some of the techniques here.

3.1 Bulk growth techniques

3.1.1 EFG growth technique

The most reliable and established technique for gallium oxide is EFG, if bulk size and quality are considered. In an iridium crucible, high purity gallium oxide source is emptied and heated in the presence of nitrogen and oxygen by RF induction coil. Capillary forces raise the melt when an iridium die with a narrow slit is dipped into molten gallium oxide and single crystals can be pulled out using a seed gallium oxide crystal. The major impurities for gallium oxide is silicon and iridium and silicon induces natural n-type activity in gallium oxide hence silicon dioxide can be used as an n-type dopant for gallium oxide, along with tin oxide as tin also increases the carrier concentration in gallium oxide. Deep acceptors in gallium oxide like magnesium and iron also play a role in the natural conductivity. The single crystals thus obtained have to be annealed at high temperatures ($> 1300^{\circ}$) for the carrier concentration in the bulk to be activated, then these can be cut into wafers for commercialization.

3.1.2 Czochralski Process

Cylindrical single crystals of gallium oxide is grown using the pulling growth process called czochralski process. It is called the pulling method, since the material is melted into an ingot and with the help of a seed crystal the melted material is pulled up while rotating the crucible for a smooth transition, and instead of pulling the seed, the crucible can also be lowered so as to fake the act of pulling but still get the same result. In fact the latter method of rotating the crucible while lowering it down is the most used form of CZ process. In the case of gallium oxide, the crucible generally used for this method i.e. iridium crucible has an interesting problem. Iridium crucibles are prone to oxidation when at high temperatures and oxygen being an integral part of the material it is considered to have parasitic effects of

creating oxygen vacancies. The presence of oxygen is crucial in obtaining a good quality single crystal of gallium oxide, having an oxygen atmosphere will inadvertently decrease the quality of the output by affecting the crucible, hence a better solution would be to use carbon-di-oxide atmosphere for the growth of gallium oxide using CZ process. This of-course will increase the cost of the set up involved in this process.

3.1.3 Floating zone process

This was the most used process when gallium oxide was grown as a substrate for other materials, since it was relatively easy process. Using FZ process the single and polycrystals were grown as rods of 10mm in diameter. This was good enough to carry out basic experiments to determine the structural properties of gallium oxide, but the requirement of current application will not be satisfied using this method, since even though the growth rates are typically 10mm/hr the maximum length grown is 50mm with a maximum diameter of 25mm. Hence researchers have moves to other bulk growth techniques.

3.2 Thin film growth techniques

3.2.1 Metalorganic chemical vapour deposition

As the name suggests the precursor for gallium used in this method is a metal-organic compound, and predominantly trimethylgallium (TMG) is used, though others precursors have been tested, but not in major use. Oxygen precursors included oxygen, ozone and water vapour, though the presence of hydrogen did suggest a lowering in the oxygen vacancy deficiencies found in gallium oxide the predominantly used precursor is oxygen, since it can also be used as the atmosphere. The carrier gases tested for gallium oxide growth are nitrogen and and argon and are found to give reliable results. The atmospheric temperature and pressure are typically around 700°C and 20 Torr and the reactor pressure

is usually 15 mTor. Water vapour as the oxidant surprisingly gave the the best single crystals of gallium oxide. They were grown hetero-epitaxially until the melt based processes discussed above paved way for affordable homo-epitaxial growth.

3.2.2 Molecular beam epitaxy

The major drawback in MBE was that pure ozygen cannot be used as an oxygen source since the evaporation rate is high, hence the sources researchers have turned are plasma and ozone. Ozone growth system had a better growth rate compared to the plasma system. Though doping can be done in MBE using Si or Sn atoms precise control is hard owing to the high pressure involved in this process. The desirable deposition temperatures were around 750°C. Sn is the preferred dopant, and the role of Ga_2O in the process of obtaining a high quality gallium oxide crystal is crucial, since they slow the process of growth and must be avoided by changing the growth conditions. Heterostructures involving gallium oxide were grown using RF-MBE and has some promising results which would lead to high performance electrical devices.

3.2.3 Halide vapour phase epitaxy

Among the thin film growths HVPE is considered to be the most desired technique for bulk growth of epitaxial gallium oxide wafers. The precursors used for gallium and oxygen are Gallium chloride and oxygen, while the carrier gas used is nitrogen. The compound GaCl is chemically processed in the chamber by flowing chloride gas over gallium metal using nitrogen as carrier and once inside the growth chamber, oxygen and gallium chloride react at an even higher temperature to form gallium oxide substrates and had an highest growth rate of 20μm/hr. No matter what the process gallium oxide

is always unintentionally doped, which raises questions about the earlier suggestion that gallium oxide be used as an oxide or dielectric in device fabrication.

CHAPTER 4

GALLIUM OXIDE : APPLICATIONS

The multitude of properties of gallium oxide makes it find applications in several different industries. It can be used as a gas sensor device owing to its oxygen vacancies, or can be used in ultraviolet photodetection and ultraviolet optoelectronics because of its ultra-wide bandgap, but it is predominantly developed for the possibility of its application in power electronics.

4.1 Gas Sensors

Since β-Ga_2O_3 is naturally n-type and the polycrystalline film's conductivity is inversely proportional to oxygen pressure in the immediate surrounding and at high temperature these vacancies are activated. The variation induces change in conductivity, hence an increase in the conductivity can be attributed to the absence of oxygen in the atmosphere. For low pressure the changes are abrupt in conductivity, where even a phase transition was suggested. At higher temperatures, the oxygen sensitivity decreases, therefore it can be used to detect gases such as hydrogen which have a reducing nature. A schottky diode based hydrogen sensor was also fabricated and tested, based on the understanding that the barrier height reduces as hydrogen gas concentration is increased. These gas sensors based on polycrystalline gallium oxide are competent only at high temperatures ($>550^{\circ}$C).

4.2 Power applications

As it was mentioned previously, the predominant research on gallium oxide is done towards the field of power electronics. Important components of power conversion are two types of devices, switching

transistors and rectifying diodes. The former controls the 'on' and 'off' states of current conduction and the latter controls the current flow direction. The conduction loss corresponds to resistive dissipation and the switching loss is controlled by capacitive components and these two contribute to total energy loss in power switching devices. The critical electric field is estimated for β-Ga_2O_3 from the empirical relation provided by Hudgins et al., (15) as 8 MV/cm. The expression for critical field and BFOM are given as,

$$E_c = 1.73 \times 10^5 (E_g)^{2.5}, \tag{4.1}$$

$$BFOM = \varepsilon \mu E_g^3 \tag{4.2}$$

From the above relation of BFOM, we can see that the value for β-Ga_2O_3 will be large since it is proportional to the cube of the bandgap, which is very large for this material. These values for β-Ga_2O_3 are nearly five times larger than both SiC and GaN, which are dominating the current power semiconductor industry. The theoretical limit of the breakdown field and the on-resistance vs breakdown voltage is shown in Fig. 5. The only shortcoming of β-Ga_2O_3 is its thermal conductivity, which will greatly affect its prospects as a power device since the cost of dissipating the heat will outcast the cost of reduction in power performance. But, if effective heating methods are developed and powerful heats sinks are designed for β-Ga_2O_3 device then it will be a viable competitor to the other power semiconductor materials, since the major requirements of a power semiconductor are,faster recovery time while switching, off-state leakage should be low, breakdown voltage should be high, low on-

resistance and should be able to operate in high temperature, i.e. heat dissipation must be fast, which is not in the case of β-Ga_2O_3, but all the other requirements are met. Device breakdown is one of the predominant requirement as noted earlier, hence understanding the phenomena causing the breakdown is equally important so effective mathematical models can be derived to solve real world problems. The focus of the next section will be on this phenomena.

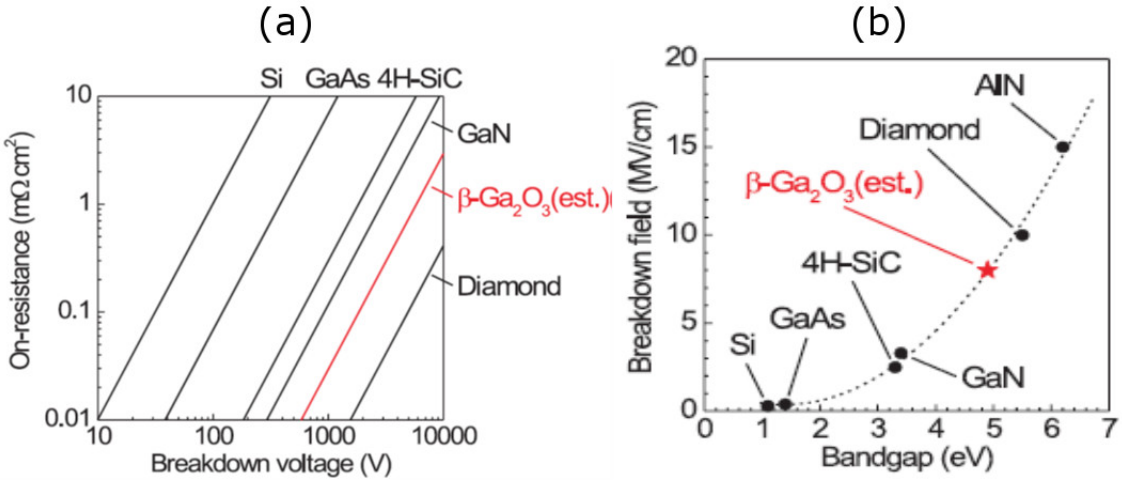

Theoretical breakdown field and On-resistance vs breakdown voltage from Ref. (2).

Figure 5: Breakdown field and on resistance

CHAPTER 5

BREAKDOWN PHENOMENA

The breakdown in a semiconductor device can happen in the following ways Impact ionization, Gate Leakage, Drain-to-source punch-through and Vertical current leakage. Gate leakage takes place when the dielectric or the oxide layer of the device is very thin that the electrons start tunnelling through the oxide and into the gate. This is increasing to be a major problem since the feature size of the devices are reducing at a pace predicted by moore's law and also since the devices are becoming thinner to save power by reducing the voltage of operation, the tunnelling is becoming a major problem. Drain-to-source punch-through happens when the space charge region surround the gate and the drain overlap each other, again following moore's law the channel length is reduced to nanometers in current devices. These two phenomenon can be tackled by altering the dimensions of the device but, impact ionization depends predominantly on the applied electric field strength which translates to the field strength at the space charge region. hence, impact ionization becomes the predominant force in determining the breakdown voltage in semiconductors.

5.1 Impact ionization

Ionization is the process of an atom becoming an ion by either losing and electron or gaining an electron and carrying a positive or a negative charge as a particle. The energy required for such an event to take place is called the ionization energy (E_i) of that particular atom and it depends on the atomic attraction of the electron to its nuclei. Usually the ionization process is explained using the dissolution

of the sodium chloride crystals into water, and how the sodium and chloride atoms become positive and negative ions respectively. Similarly, impact ionization occurs in gases and solids when an highly energised electron collides into an atom creating an electron and hole pair and loses some energy. Since the system is in non equilibrium by considering that the generation processes' rate is much larger than the recombination process, the electrons generated are kept at an highly energised state. This leads to the fact that, the one electron that created an electron hole pair, joins the other electron and these two electrons now create a new electron hole pair each, hence bringing the tally of total ionised electrons as four and the number of newly created electron-hole pair is two. This process repeats itself ionizing more atoms and creating more free electron hence this process is called a charge generation mechanism. The number of particles involved in this process include the high energy electron, the electron to be knocked off and the atom to be ionised making it a three-body or particle ionization process, which draws parallel to the sun, earth and the moon three body problem.

Impact ionization can only occur when this freed electron gains enough energy equal to the threshold energy of ionization, which can be approximated to $E_i = 1.5 \times E_g$, where E_g is the energy bandgap of the semiconductor. The occurrence of impact ionization can be determined by measuring the bulk current in a device and the rate at which these ionizations happen is called the ionization rate (α). The exact definition is "the number of electron-hole pairs generated by a carrier per unit distance" is called the ionization rate. This ionization rate depends on the probability that a carrier reaches the ionization energy.

Let us consider a simple semiconductor device, a p-n junction diode, breakdown occurs when excessive current flow occurs at the junction breaking the space charge region. Consider the gradient of

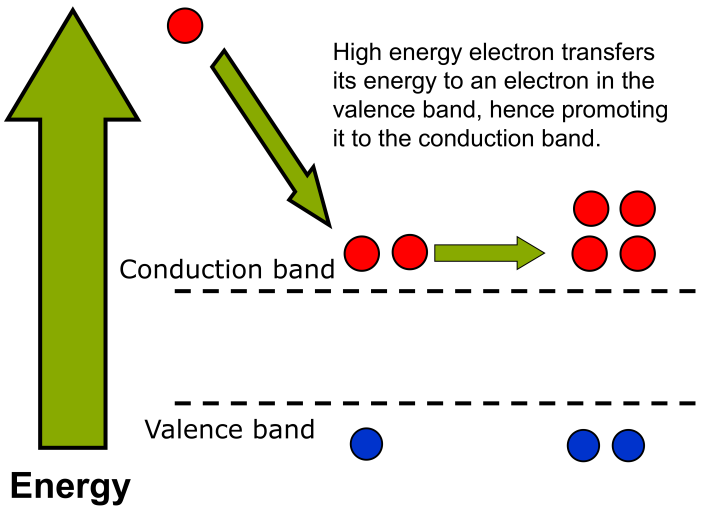

The process of Impact ionization explained in the sketch.

Figure 6: Impact ionization process

electric field in the space charge region and an electron is generated at the border of this region. As the electron moves towards the junction it gains energy, and when it gains enough energy and crosses the threshold energy then collision made by it will generate an electron hole pair. Now this probability that the electron reaches the threshold energy has been determined by Wolff, Shockley and Baraff in three different approaches.

5.1.1 Shockley approach

Shockley approaches this problem in a very straight forward way by saying that the only electron that reach this ionization energy are those that are 'lucky' enough to avoid collisions until they have enough energy to knock down an electron from an atom. This very simple but effective approach is given by the relation,

$$\alpha \propto exp(\frac{-E_i}{q \cdot l \cdot E}) \tag{5.1}$$

where, l is the mean free path between collision due to scattering, E is the applied field strength, q is the charge of an electron. We can see that in this approach ionization rate depends on those electrons that are fortunate enough to escape collision and hence is called the "lucky electron model".

5.1.2 Wolff approach

Wolff takes a different approach that is quite opposite to that of Shockley, he assumes a diffusion approximation. In diffusion approximation, electron gains energy at a steady pace over time, going through many collision in the process and finally reaching enough energy to create an electron hole pair. The relation between ionization rate and electric field strength in this approach is given by,

$$\alpha \propto exp(\frac{-a}{E^2}) \tag{5.2}$$

where, a is a constant determined by the material properties and measured using experiments and E is the applied electric field strength.

5.1.3 Baraff approach

Baraff's approach combined the positives of the previous two approaches and eliminated the weaknesses of them both. Baraff considered the collision density and derived an integral to calculate the same and used it in determining the Townsend's alpha α or the ionization rate. By taking such an approach, he inevitably derives a relationship between three independent parameters, the threshold energy, energy loss per phonon collision or the optical phonon energy and the mean free path and considers both the mean free path due to scattering of electrons (or impact ionization scattering) and the phonon mean free path to be constant and same. Baraff's approach has the following relation,

$$\alpha \cdot \lambda = f\left(\frac{E_r}{E_i}, \frac{E_i}{q \cdot \lambda \cdot \mathbf{E}}\right), \tag{5.3}$$

where, α is the ionization rate, λ the phonon mean free path, E_r the optical phonon energy, E_i the ionization energy. The universal plot given by Baraff for the ionization rate for all semiconductors is given in Fig. 7

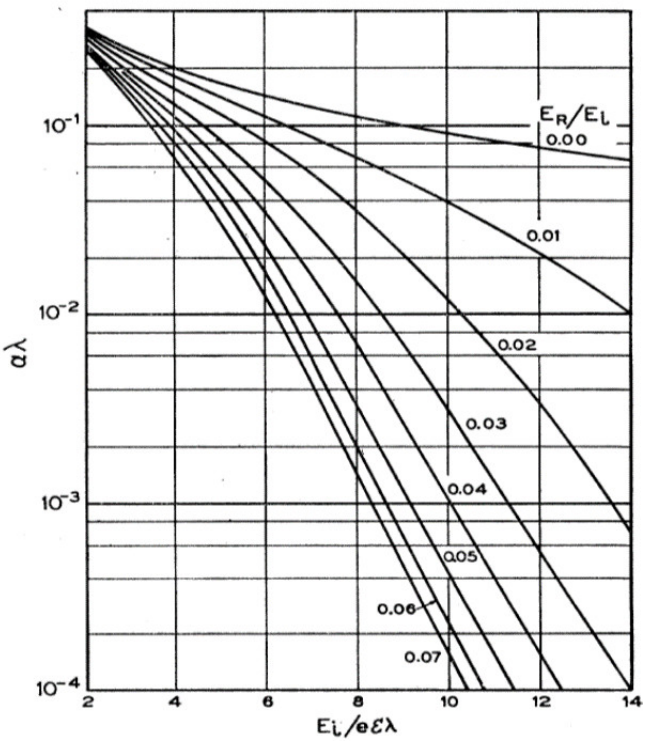

Baraff's universal plot of ionization rate vs applied electric field for all semiconductors.

Figure 7: Baraff's Universal plot

CHAPTER 6

CRITICAL MULTIPLICATION RATIO

The models described above are pseudolocal in nature, that is to say the ionization rate calculated depends only on the electric field strength applied but not on the position where the carriers are generated, and suggests that the models can be used for any position within the space-charge region. Such a description assumes an unphysical situation where the non-ionized carriers theoretically have negative values within the device for structures with sufficiently high multiplication. A critical multiplication ratio (M_c), between ionized and total number of carriers at a any position in the structure, was suggested by Okuto and Crowell in Ref. (16), to address this issue in their non-localized concept description of avalanche ionization effect, which is given by,

$$M_c = \frac{2[1+\alpha_r(\mathbf{E})D]}{\alpha_a(\mathbf{E})D[2+\alpha_r(\mathbf{E})D]} \tag{6.1a}$$

with:

$$\alpha_a(\mathbf{E}) = \frac{\alpha_r(\mathbf{E})[1+\alpha_r(\mathbf{E})D]}{1+4\alpha_r(\mathbf{E})D+2\alpha_r^2(\mathbf{E})D^2}, \tag{6.1b}$$

$$\alpha_r(\mathbf{E}) = [X-D]^{-1}, \tag{6.1c}$$

$$D = \frac{E_i - N_r E_r}{q\cdot\mathbf{E}}, \tag{6.1d}$$

$$X = Dexp(((D/\lambda_r)^2 + [0.217(E_i/E_r)^{1.14}]^2)^{1/2} - 0.217(E_i/E_r)), \tag{6.1e}$$

where N_r is the net number of optical phonons absorbed by the carrier and is assumed as zero, since only absorption of energy is considered at low temperatures. X, is the average distance at which an ionizatoin scattering occurs, D, is the dark-space distance, $\alpha_r(\mathbf{E})$ is the non-localized single-carrier ionization probability, $\alpha_a(\mathbf{E})$ is the "apparent ionization coefficient" introduced in Ref (16) to explain pseudo-local approximation in the description of the ionization effect in semiconductors using the non-localized concept. The expression for M_c has the following theoretical limits,

$$Mc \to \frac{1}{\alpha_a(\mathbf{E})D} \quad when \quad \mathbf{E} \to 0 \tag{6.2a}$$

$$Mc \to 4 \quad when \quad \mathbf{E} \to \infty. \tag{6.2b}$$

CHAPTER 7

APPROXIMATIONS FOR BARAFF'S UNIVERSAL PLOT

Several approximations have been suggested for baraff's universal plot. Though it has a good conceptual representation, the relation given by baraff cannot be used for the purpose of simulation. For simulation, we need concrete, tangible values and hence these approximations are proposed either empirically or through fitting of the baraff curve experimentally. The major approximations available are, Crowell-Sze approximation, Thornber approximation and Sutherland approximation

7.1 Selberherr IIM

Several Impact Ionization models are used for the determination of breakdown voltage in TCAD simulations, of which Selberherr model (17) is the most appropriate for β-Ga_2O_3 since it allows for the maximum customization of its coefficients for the purpose of TCAD simulations. The model is given by the following expression,

$$\alpha = \alpha_0 \cdot \exp\left(-\left(\frac{E^{crit}}{\mathbf{E}}\right)^{\beta}\right), \tag{7.1}$$

where, α is the Ionization rate, α_0 the impact ionization rate constant, E^{crit} is the critical electric field, $\mathbf{E}$ is the applied electric field strength at a specific position along the current flow direction and β, a fitting constant, is in the range $[1,2]$. We have considered the values of electrons for holes too since p-type has not been developed for β-Ga_2O_3 at present. To estimate the coefficients for Selberherr's IIM,

the approximation methods provided by Crowell-Sze, Sutherland and Thornber are used to fit Baraff's universal plot (18) for ionization rate, given by Eqn. 5.3.

7.1.1 Crowell-Sze approximation

The Baraff curve approximation proposed by Crowell and Sze (19) is expressed as,

$$\alpha \cdot \lambda = \exp\left(R_0 + R_1 \cdot x + R_2 \cdot x^2\right), \tag{7.2a}$$

with:

$$R_0 = -1.92 + 75.5 \cdot r - 757 \cdot r^2, \tag{7.2b}$$

$$R_1 = 1.75 \cdot 10^{-2} - 11.9 \cdot r + 46 \cdot r^2, \tag{7.2c}$$

$$R_2 = 3.9 \cdot 10^{-4} - 1.17 \cdot r + 11.5 \cdot r^2, \tag{7.2d}$$

where,

$$r = \frac{E_r}{E_i}, \tag{7.2e}$$

$$x = \frac{E_i}{q \cdot \lambda \cdot \mathbf{E}}. \tag{7.2f}$$

This approximation is accurate over the range r $\in [0.01, 0.06]$ and x $\in [5, 16]$ within two percent maximum error.

7.1.2 Sutherland approximation

A more rigorous approximation was proposed by Sutherland (1) given by,

$$\alpha \cdot \lambda = \exp(R_0 + R_1 \cdot x + R_2 \cdot x^2 + R_3 \cdot x^3), \tag{7.3a}$$

with:

$$R_0 = -7.238 \cdot 10^{-2} - 51.5 \cdot r + 239.6 \cdot r^2 + 3357 \cdot r^3, \tag{7.3b}$$

$$R_1 = -0.4844 + 12.45 \cdot r + 363 \cdot r^2 - 5836 \cdot r^3, \tag{7.3c}$$

$$R_2 = 2.982 \cdot 10^{-2} - 7.571 \cdot r - 148.1 \cdot r^2 + 1627 \cdot r^3, \tag{7.3d}$$

$$R_3 = -1.841 \cdot 10^{-5} - 0.1851 \cdot r + 10.41 \cdot r^2 - 95.65 \cdot r^3. \tag{7.3e}$$

For the range r $\in [0.01, 0.07]$ and x $\in [3, 14]$ this approximation is expected to fit Baraff's curve perfectly.

7.1.3 Thornber approach

The empirical expression proposed by Thornber (20) has been consistent with an elaborate momentum and energy scaling theory and is given by,

$$\alpha = \frac{\mathbf{E}}{E_i} \cdot \exp\left(- \frac{B_j}{\frac{k \cdot T \cdot B_j}{E_i} + \mathbf{E} + \frac{E^2}{B_r}} \right), \tag{7.4a}$$

where,

$$B_j = \frac{E_r}{q \cdot \lambda}, \tag{7.4b}$$

$$B_r = \frac{E_i}{q \cdot \lambda}. \tag{7.4c}$$

B_j is the threshold field at which the ionization energy is reached in one mean free path and B_r is when phonon energy is reached in one mean free path. To determine the value of impact ionization rates from the above expressions, we need to determine the value of optical phonon mean free path (MFP), on which not much experimental or theoretical research has been done and no data is available for β-Ga_2O_3.

CHAPTER 8

PHONON MEAN FREE PATH

Phonons are crystal or lattice vibrations. They can be classified as acoustic phonons and optic phonons based on the vibrating ion's phase difference. When two atoms vibrate out of phase, the atoms move towards each other or away from each other, it is considered as optic phonons and when they vibrate in phase, the atoms move together vertically or horizontally, it is considered acoustic phonons. The word optic and acoustic by themselves do not mean that the optic phonons are in the visible spectrum but is simply defined as such because of the frequency difference. The optic phonons have higher frequency and the acoustic phonon has lower frequency than the optic and hence also have lesser energy compared to optical phonons.

The phonon mean free path is the distance a particle has travelled after encountering a phonon and before coming in contact with another phonon. Since phonon is not a particle a good way of understanding the concept of phonon mean free path is to consider a rod kept at different temperatures at the ends, the thermal conduction is not immediate i.e. the conductivity is not infinite, hence a the introduction of a mean free path to describe a phenomenon such as mean free path. The mean free path of phonons depend on depend on two variables, scattering rate among phonons and the scattering rate with impurities and boundaries of the crystal. The value of MFP can be determined from its relation to thermal conductivity and specific heat capacity provided as gray's approximation, where only the scattering due to phonons are considered at temperatures higher than 300°K,

$$\kappa \simeq \frac{1}{3} \cdot v_{ph} \cdot \lambda_{ph} \cdot c_v, \tag{8.1}$$

where κ is the thermal conductivity, v_{ph} is the phonon group velocity (values for v_{ph} is available in Ref (21)), λ_{ph} is the phonon mean free path, which needs to be determined, c_v is the specific heat capacity which is calculated using the Debye model of specific heat represented as,

$$C_v = 3Nk\frac{3}{x_D^3}\int_0^{x_D} \frac{x^4 e^x}{(e^x-1)^2} dx, \tag{8.2}$$

where, $x_D = \frac{\theta_D}{T}$ and θ_D is the Debye temperature, which can take the experimentally measured value of 738°K (21) or the first principles estimate of 872°K (22) for β-Ga_2O_3, T is the absolute temperature, k is the Boltzmann constant and N is the number of atoms, considered as avogadro's number.

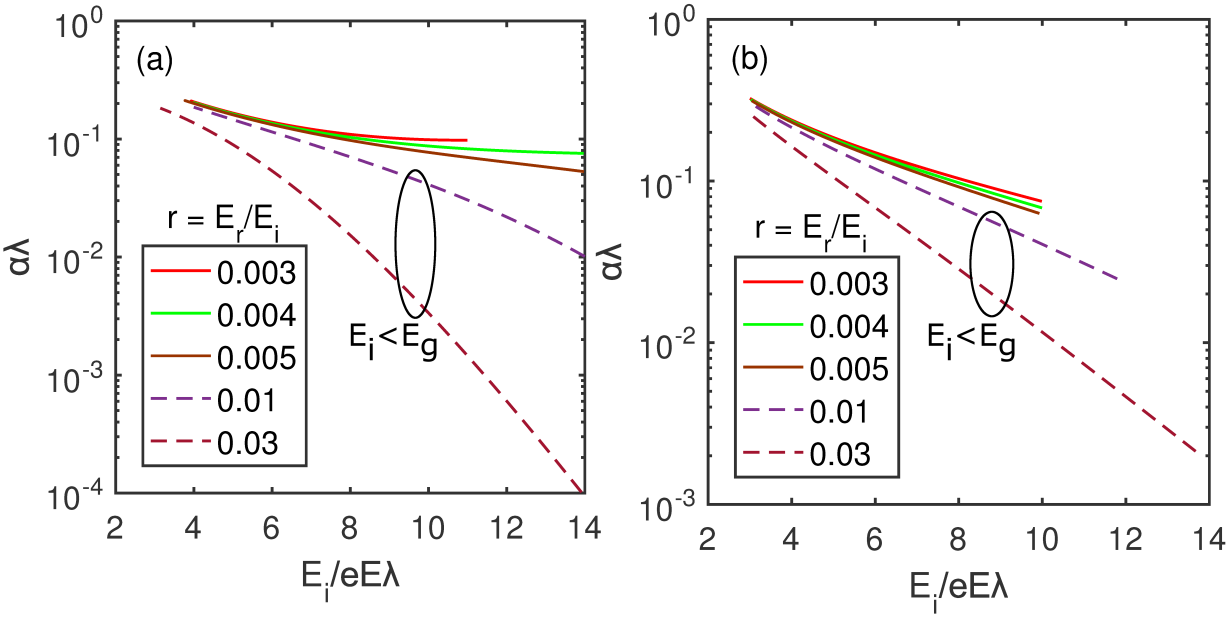

The numerically obtained baraff plots for Ionization rates in β-Ga_2O_3 along the [010] direction using Sutherland model (figure on the left panel) and Thornber model (figure on the right panel). The plots were obtained for different values of ionization energy (E_i), including values extended below E_g (plotted as dashed lines) to show that the obtained curves fit the universal baraff plot for semiconductors.

Figure 8: Baraff Curves for β-Ga_2O_3

TABLE I: THERMAL CONDUCTIVITY AND PHONON GROUP VELOCITY.

Crystallographic direction	Thermal Conductivity $(W/m-K)$	Phonon group velocity(L_A) $\left(10^5 cm \cdot s^{-1}\right)$
[010]	27± 2.0	7.8
[100]	14.7±1.5	5.4
[001]	13.3±1.0	7.1
$[\bar{2}01]$	10.9±1.0	6.6

Values are for β-Ga_2O_3.

CHAPTER 9

RESULTS AND DISCUSSION

In order to estimate the impact ionization rates we first determine the value for optical phonon mean free path (MFP,λ_{ph}) using Eq. 8.1 where the values of thermal conductivity, phonon group velocity and specific heat capacity are listed in Table I. Owing to anisotropy in the crystal structure, the approximate values of λ_{ph} are obtained for different crystallographic directions as catalogued in Table II and these estimates are justified when we compare the thermal conductivities of β-Ga_2O_3 and GaN given as 27 and 230 (23) W/m-K, respectively. The phonon group velocity of GaN is determined to be in the range 6.9-8.2$\times$ $10^5 cm\cdot s^{-1}$, (24) the specific heat is estimated to be 0.49 $J\cdot g^{-1}\cdot^{\circ}C^{-1}$, (25) correlating these values to those of β-Ga_2O_3, 7.8$\times$ $10^5 cm\cdot s^{-1}$ and 0.56 $J\cdot g^{-1}\cdot^{\circ}C^{-1}$ (26) (for [010]) and using Eq. (8.1) we see that the phonon mean free path is the only variable affecting thermal conductivity and has to be larger in GaN than β-Ga_2O_3, in fact λ_{ph} of GaN is larger by an order of 10 from Ref (27). It is important to note that the λ_{ph} thus obtained is for the acoustic branch and can still be used to determine the ionization rate for the following reason. We consider a situation where no acoustic phonons are present and if the energy of the electron is below the optical phonon energy, the mean free path will be infinite since no collision will take place unless the electron gains energy above match the optical phonon energy in order to be considered for scattring, hence the presence of the acoustic phonons give a minimum value for λ_{ph} beyond which it cannot increase, and this estimation will be a good approximation for the purpose of calculating the ionization coefficient. The value of λ_{ph} is estimated as 5.2604 Å for β-Ga_2O_3, and E_r is derived from Ref. (28) to be 24.81 meV.

Baraff adopts an approach which neither relies on diffusion approximation followed by Wolff (29) nor Shockley's (30) "spike" distribution to describe electron transport but rather derives an integral equation for the collision density in order to estimate ionization rates, for all semiconductors. The curves from the mathematical models discussed in section 7.1 must fit this universal plot provided by Baraff for different values of ionization energy (E_i) over a range of applied electric field strength ($\mathbf{E}$), and the values to which they fit for β-Ga_2O_3 are given in Table II. The baraff plots illustrated are for Sutherland model, Fig.8(a), and Thornber model, Fig.8(b) from which we can observe that Sutherland model fits more perfectly and for a higher range than Thornber, hence the values of ionization rate (α) and applied electric field strength $(\mathbf{E})$ are calculated using this model. The dashed lines, for values of E_i below E_g, are shown to clarify the baraff curve fitting of the models under study and solid lines are for E_i above E_g. These curves also give the range in which the values for ionization rate, α, and applied electric field strength $(\mathbf{E})$ are reliable for the material under consideration. The plot for the model provided by Crowell-Sze is not shown. The figures are plotted only for $[010]$, since the thermal conductivity is maximum along this direction. The estimates of the coefficients α and $(\mathbf{E})$ is extracted from Fig. 9(a) (ionization coefficient *vs* inverse electric field) and Fig. 9(b) $((log - log)$ plot) respectively, and the ionization rate constant α_0 can be calculated from these values using Eq. (7.1). The values of λ_{ph}, E_r and E_i used to plot Fig. 9 are 5.2604Å, 24.81 meV and 7.275 eV ($1.5\times$ E_g), respectively. There are no experimental verifications available for ionization rates of β-Ga_2O_3. The predicted values are listed in Table. II and given the large energy band gap of β-Ga_2O_3, the value estimated for applied electric field strength can be justified when juxtaposed with other wide-bandgap semiconductors.

A comparison of $\alpha(vs)\mathbf{E}$ plots between major wide-bandgap semiconductor materials considered for power electronics can be derived from Fig. 10 where the curves were traced using the variables described in section 7.1 with parameters from Ref. (27; 23; 25; 31; 24) for GaN, Ref. (32; 33; 34; 35) for 4H-SiC. The field strength range between which ionization occurs is larger in β-Ga_2O_3 than GaN or 4H-SiC and a similar comparison can be made for materials Germanium, Silicon, Gallium Arsenide and Gallium Phosphide from Ref. (36). The difference in field strength is attributed to the bandgap of the material since the field strength required for ionization increases as the bandgap increases. The ionization rate depends on the values of λ_{ph} and E_r which determine, the average distance a carrier has to travel to acquire high energy and the ratio of "cross section" (r) for ionization respectively, ergo comparing these values to GaN and 4H-SiC predicts the ionization rate to be higher in β-Ga_2O_3, as estimated. The critical multiplication ratio M_c discussed in section 7.1 aids in understanding the limitations of the ionization models and the numerically calculated M_c is shown in Fig. 11. If the ratio of the total number carriers to the ionized carrier is higher than M_c then the models do not hold and if it is lower the boundary conditions are important. We can see that value of M_c is large at low field and saturates at high field as predicted by the theoretical limits and also notice that the field strength at which the multiplication holds is high and compliments the field strength obtained from baraff plots.

TABLE II: IMPACT IONIZATION VALUES.

Crystallo graphic direction (Material)	Impact Ionization rate (α) [$\times 10^6 cm^{-1}$]	Critical Electric Field (E^{crit}) [$\times 10^8 V cm^{-1}$]	Phonon Mean Free Path (λ)[Å]	Applied Electric Field($\mathbf{E}$)[$\times 10^7 V cm^{-1}$]
[010]	3.98	0.921	5.260	1.43-4
[100]	7.626	1.581	3.067	3.37-7.7
[001]	8.965	1.622	2.99	3.08-9.2
[$\bar{2}$01]	9.485	1.755	2.763	3.5-9.7
(GaN)	0.25	0.34	58	0.12-0.53
(4H-SiC)	0.15	0.16	32.5	0.09-0.35

Impact ionization coefficients for different crystallographic directions of β-Ga_2O_3. Values of GaN (from Ref. (27; 23; 25; 31; 24)) and 4H-SiC (from Ref. (32; 33; 34; 35)) is given for comparison.

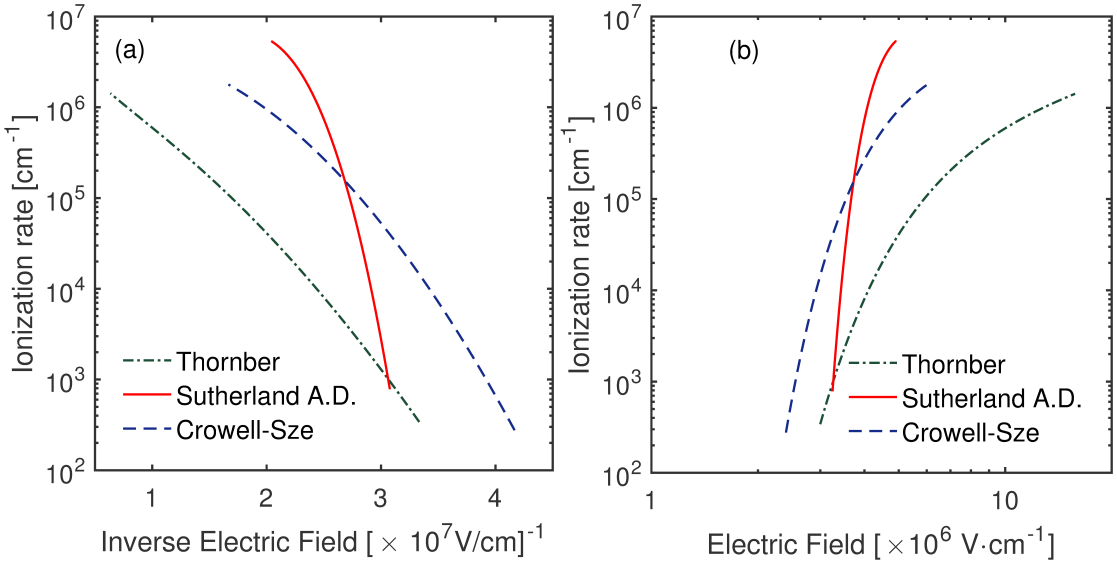

The theoretically calculated ionization rate curves (α) for β-Ga_2O_3 at 300°K along the [010] direction for all three methods. The rates calculated are for both electrons and holes. The figure on the left panel gives the ionization coefficient (α) as a function of inverse electric field, from where the ionization coefficient is derived and the figure on the right panel shows the Ionization rate (α) as a function of electric field from which the applied electric field strength range is obtained. The previously determined ionization rate is valid within this range.

Figure 9: Ionization rate curves for β-Ga_2O_3

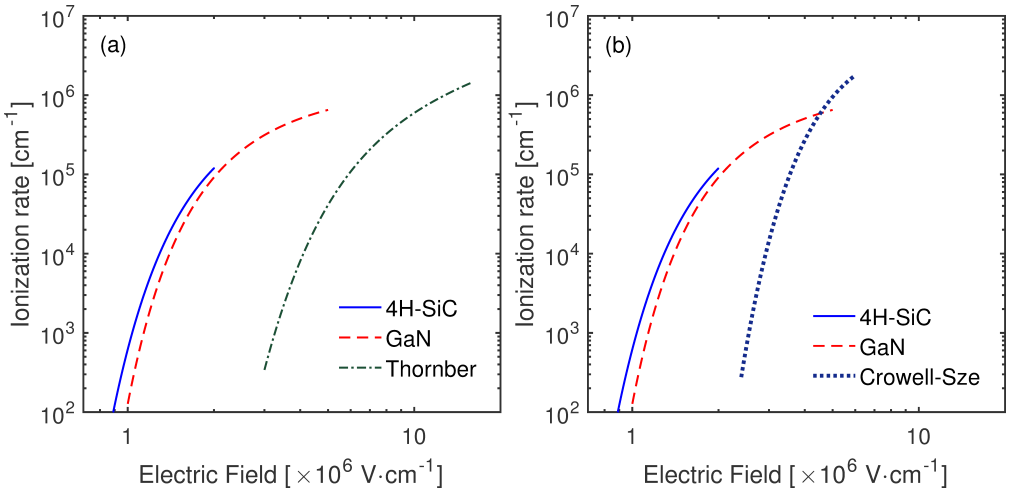

Ionization rate curves for 4H-SiC, GaN and β-Ga_2O_3. Comparison of the curves suggests that the electric field strenght predominantly depends on the bandgap and the predicted ionization rate would be higher in β-Ga_2O_3. The curves for GaN were traced using parameters from references (27; 23; 25; 31; 24) and for 4H-SiC from (32; 33; 34; 35). The ionization rate plot of GaN was extrapolated for clarity.

Figure 10: Ionization rate comparison with 4H-SiC and GaN

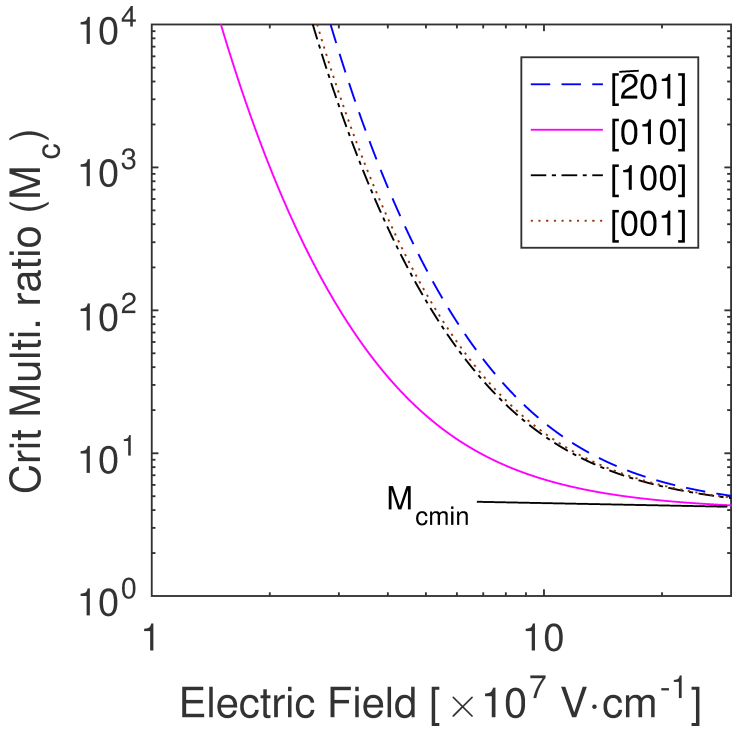

The critical multiplication ratio (M_c) as a function of electric field, for both electrons and holes, along the four crystallographic directions at 300°K. M_{cmin} denotes the theoretical minimum value for M_c at infinite field. M_c is the ratio of the total number of carriers (electrons + holes) to the number of electrons (or holes). If the ratio of the total number of carriers to the number of ionized carriers is higher than M_c the approximations do not hold.

Figure 11: Critical multiplication ratio.

CHAPTER 10

CONCLUSION

We have estimated the ionization coefficients of β-Ga_2O_3 using approximation models provided by Crowell-Sze, Thornber and Sutherland, for Baraff's universal plot of ionization rates in semiconductors. The phonon mean free path was estimated using Gray approximation of thermal conductivity and debye's model was used to determine specific heat. The ionization rate curves thus determined were compared with other major power semiconductors (GaN and 4H-SiC), and it was found that as the bandgap increases the field strength required for ionization also increases, regardless of phonon energy. Values for critical multiplication ratio of the carriers was determined to address the pseudolocal nature of the approximations. A plot for the same is illustrated and above these values the models do not hold.

The ionization rate constant can be determined by measuring the breakdown voltage and the electric field at this breakdown. Using the measured applied field, in the expression for ionization rate, we can deduce the ionization rate constant. Alternatively, existing breakdown values of gallium oxide devices can be used, provided we know the crystal orientation of the channel of the device during breakdown. Then this device can be simulated for the suggested range of values of ionization rate until the measured breakdown voltage is obtained. Finally, the ionization rate constant can be calculated using its relation to ionization rate and applied electric field.

The approximation models considered here though developed based on silicon and gallium arsenide holds true for a wide bandgap semiconductor, such as gallium oxide, since the carrier density approach by Baraff is universal for all semiconductors. The dependence of ionization rate to the change in carrier

concentration was not considered. An experimental analysis measuring I_d-V_d characteristics of β-Ga_2O_3 MOSFET, such as in Ref. (37), will assist in verifying the estimated ionization coefficient values.

CITED LITERATURE

1. Sutherland, A.: An improved empirical fit to baraff's universal curves for the ionization coefficients of electron and hole multiplication in semiconductors. IEEE Transactions on Electron Devices, 27(7):1299–1300, 1980.

2. Higashiwaki, M., Sasaki, K., Kuramata, A., Masui, T., and Yamakoshi, S.: Gallium oxide (ga2o3) metal-semiconductor field-effect transistors on single-crystal β-ga2o3 (010) substrates. Applied Physics Letters, 100(1):013504, 2012.

3. Jessen, G., Chabak, K., Green, A., McCandless, J., Tetlak, S., Leedy, K., Fitch, R., Mou, S., Heller, E., Badescu, S., et al.: Toward realization of ga 2 o 3 for power electronics applications. In Device Research Conference (DRC), 2017 75th Annual, pages 1–2. IEEE, 2017.

4. Roy, R., Hill, V., and Osborn, E.: Polymorphism of ga2o3 and the system ga2o3h2o. Journal of the American Chemical Society, 74(3):719–722, 1952.

5. Geller, S.: Crystal structure of β-ga2o3. The Journal of Chemical Physics, 33(3):676–684, 1960.

6. Åhman, J., Svensson, G., and Albertsson, J.: A reinvestigation of β-gallium oxide. Acta Crystallographica Section C: Crystal Structure Communications, 52(6):1336–1338, 1996.

7. Bradley, C. and Cracknell, A.: The mathematical theory of symmetry in solids: representation theory for point groups and space groups. Oxford University Press, 2010.

8. Aroyo, M. I., Kirov, A., Capillas, C., Perez-Mato, J., and Wondratschek, H.: Bilbao crystallographic server. ii. representations of crystallographic point groups and space groups. Acta Crystallographica Section A: Foundations of Crystallography, 62(2):115–128, 2006.

9. Aroyo, M. I., Perez-Mato, J. M., Capillas, C., Kroumova, E., Ivantchev, S., Madariaga, G., Kirov, A., and Wondratschek, H.: Bilbao crystallographic server: I. databases and crystallographic computing programs. Zeitschrift für Kristallographie-Crystalline Materials, 221(1):15–27, 2006.

10. Aroyo, M. I., Perez-Mato, J., Orobengoa, D., Tasci, E., De La Flor, G., and Kirov, A.: Crystallography online: Bilbao crystallographic server. Bulg. Chem. Commun, 43(2):183–97, 2011.

11. Aroyo, M. I., Orobengoa, D., de la Flor, G., Tasci, E. S., Perez-Mato, J. M., and Wondratschek, H.: Brillouin-zone database on the bilbao crystallographic server. Acta Crystallographica Section A: Foundations and Advances, 70(2):126–137, 2014.

12. Peelaers, H. and Van de Walle, C. G.: Brillouin zone and band structure of β-ga2o3. physica status solidi (b), 252(4):828–832, 2015.

13. Passlack, M., Hunt, N., Schubert, E., Zydzik, G., Hong, M., Mannaerts, J., Opila, R., and Fischer, R.: Dielectric properties of electron-beam deposited ga2o3 films. Applied physics letters, 64(20):2715–2717, 1994.

14. Hoeneisen, B., Mead, C., and Nicolet, M.: Permittivity of β-ga_2o_3 at low frequencies. Solid-State Electronics, 14(10):1057–1059, 1971.

15. Hudgins, J. L., Simin, G. S., Santi, E., and Khan, M. A.: An assessment of wide bandgap semiconductors for power devices. IEEE Transactions on Power Electronics, 18(3):907–914, 2003.

16. Okuto, Y. and Crowell, C.: Ionization coefficients in semiconductors: A nonlocalized property. Physical Review B, 10(10):4284, 1974.

17. Siegfried, S.: Analysis and simulation of semiconductor devices, 1984.

18. Baraff, G. A.: Distribution functions and ionization rates for hot electrons in semiconductors. Physical review, 128(6):2507, 1962.

19. Crowell, C. and Sze, S.: Temperature dependence of avalanche multiplication in semiconductors. Applied Physics Letters, 9(6):242–244, 1966.

20. Thornber, K.: Applications of scaling to problems in high-field electronic transport. Journal of Applied Physics, 52(1):279–290, 1981.

21. Guo, Z., Verma, A., Wu, X., Sun, F., Hickman, A., Masui, T., Kuramata, A., Higashiwaki, M., Jena, D., and Luo, T.: Anisotropic thermal conductivity in single crystal β-gallium oxide. Applied Physics Letters, 106(11):111909, 2015.

22. He, H., Blanco, M. A., and Pandey, R.: Electronic and thermodynamic properties of β-ga 2 o 3. Applied physics letters, 88(26):261904, 2006.

23. Jeżowski, A., Danilchenko, B., Boćkowski, M., Grzegory, I., Krukowski, S., Suski, T., and Paszkiewicz, T.: Thermal conductivity of gan crystals in 4.2–300 k range. Solid state communications, 128(2-3):69–73, 2003.

24. Truell, R., Elbaum, C., and Chick, B. B.: Ultrasonic methods in solid state physics. Academic press, 2013.

25. Levinshtein, M. E., Rumyantsev, S. L., and Shur, M. S.: Properties of Advanced Semiconductor Materials: GaN, AlN, InN, BN, SiC, SiGe. John Wiley & Sons, 2001.

26. Galazka, Z., Irmscher, K., Uecker, R., Bertram, R., Pietsch, M., Kwasniewski, A., Naumann, M., Schulz, T., Schewski, R., Klimm, D., et al.: On the bulk β-ga2o3 single crystals grown by the czochralski method. Journal of Crystal Growth, 404:184–191, 2014.

27. Danilchenko, B., Paszkiewicz, T., Wolski, S., Jeżowski, A., and Plackowski, T.: Heat capacity and phonon mean free path of wurtzite gan. Applied physics letters, 89(6):061901, 2006.

28. Kranert, C., Sturm, C., Schmidt-Grund, R., and Grundmann, M.: Raman tensor elements of β-ga 2 o 3. Scientific Reports, 6:35964, 2016.

29. Wolff, P.: Theory of electron multiplication in silicon and germanium. Physical Review, 95(6):1415, 1954.

30. Shockley, W.: Problems related top-n junctions in silicon. Czechoslovak Journal of Physics, 11(2):81–121, 1961.

31. Oğuzman, I. H., Bellotti, E., Brennan, K. F., Kolnık, J., Wang, R., and Ruden, P. P.: Theory of hole initiated impact ionization in bulk zincblende and wurtzite gan. Journal of Applied Physics, 81(12):7827–7834, 1997.

32. Choyke, W. J. and Patrick, L.: Optical properties of 4h, 6h, 15r, 21r, cubic sic. Technical report, WESTINGHOUSE RESEARCH LABS PITTSBURGH PA, 1969.

33. Berger, L. I.: Semiconductor materials. CRC press, 1996.

34. Harris, G. L.: Properties of silicon carbide. Number 13. Iet, 1995.

35. Konstantinov, A., Wahab, Q., Nordell, N., and Lindefelt, U.: Ionization rates and critical fields in 4h silicon carbide. Applied Physics Letters, 71(1):90–92, 1997.

36. Okuto, Y. and Crowell, C.: Energy-conservation considerations in the characterization of impact ionization in semiconductors. Physical Review B, 6(8):3076, 1972.

37. Higashiwaki, M., Sasaki, K., Kamimura, T., Hoi Wong, M., Krishnamurthy, D., Kuramata, A., Masui, T., and Yamakoshi, S.: Depletion-mode ga2o3 metal-oxide-semiconductor field-effect transistors on β-ga2o3 (010) substrates and temperature dependence of their device characteristics. Applied Physics Letters, 103(12):123511, 2013.

VITA

GIFTSONDASS IRUDAYADASS

Education	M.S. Electrical and Computer Engineering University of Illinois at Chicago	2015 – 2018
	B.E. Electronics and Communications Engineering Anna University	2007 – 2011
Awards	Full tuition fee waiver under the Board of Trustees Scholarship for Graduate Students, Fall 2016 Full tuition fee waiver under the Board of Trustees Scholarship for Graduate Students, Spring 2017	
Experience	Department of Electrical and Computer Engineering, University of Illinois at Chicago, Chicago, Illinois: Graduate Teaching Assistant ECE 115 Introduction to Electrical and Computer Engineering, Fall 2016	